

Imaging Self-Organized Domains at the Micron Scale in Antiferromagnetic Elemental Cr Using Magnetic X-ray Microscopy

P. G. Evans,¹ E. D. Isaacs,¹ G. Aeppli,² Z.-H. Cai,³ and B. Lai³

¹ Bell Laboratories, Lucent Technologies, 600-700 Mountain Ave., Murray Hill, NJ 07974

² NEC Research Institute, 4 Independence Way, Princeton, NJ 08540

³ Advanced Photon Source, Argonne National Laboratory, Argonne, IL 60439

ABSTRACT

The domains of antiferromagnetic order in elemental chromium can be observed with spatial resolution that is improved by orders of magnitude in comparison with previous techniques using magnetic x-ray scattering with an incident x-ray beam focused to a submicron spot. This use of magnetic x-ray microscopy takes advantage of the incommensurate spin density wave order in Cr to isolate magnetic scattering. The spin polarization dependence of the magnetic x-ray scattering cross section allows the first order spin-flip transition near 120 K to be imaged directly.

INTRODUCTION

At temperatures below the Néel transition at $T_N=311$ K, conduction electrons in metallic chromium are organized in an antiferromagnetic spin-density wave (SDW).¹ The SDW is a sinusoidal modulation over a period of tens of lattice constants of the amplitude of the alternating spin structure typical of antiferromagnets. Because the SDW period is incommensurate with the lattice, there are domains differing in the orientation of the modulation vector \mathbf{Q} . In chromium, \mathbf{Q} is constrained to be along $\langle 001 \rangle$ directions, leading to three possible domain orientations. Macroscopically observable phenomena such as anomalies in magnetic and mechanical responses¹ as well as the renewed importance of Cr layers since the development of exchange-biased magnetoresistive structures² have driven the development of a microscopic understanding of SDW domains in Cr.

MAGNETIC X-RAY MICROSCOPY EXPERIMENTS

We imaged antiferromagnetic domains in Cr using non-resonant magnetic x-ray diffraction in experiments performed at station 2ID-D of the Advanced Photon Source. The incident beam was focused to a submicron spot by a Fresnel phase zone plate with a 40 cm nominal focal length.³ Because zone plate optics produce images of the source at several orders, a 20 μm aperture in a Pt-Ir disk was used to select radiation focused to the first order spot. The sample was mounted on a four-circle x-ray goniometer for scattering from reflections along the [001] direction with the incident radiation polarized in the scattering plane. A real space map of the antiferromagnetic domain structure was produced by plotting the intensity of the magnetic scattering as the sample was scanned in a raster pattern under the beam. The x-ray scattering due to magnetic order within the sample can be isolated easily from scattering from structural periodicity because the incommensurate SDW leads to a set of six purely magnetic reflections near each forbidden Bragg reflection of the body centered cubic lattice. Near (001), for example,

these reflections are $(\pm\delta 0 1)$, $(0 \pm\delta 1)$, and $(0 0 1\pm\delta)$. In addition, the SDW leads to a strain wave with conventional charged reflections in similar locations at distances 2δ from allowed Bragg peaks. The value of δ varies from 0.04 just below T_N to 0.05 at low temperatures.⁴ The locations of these reflections in the $(0KL)$ plane of reciprocal space near (001) and (002) are diagrammed in Figure 1(a).

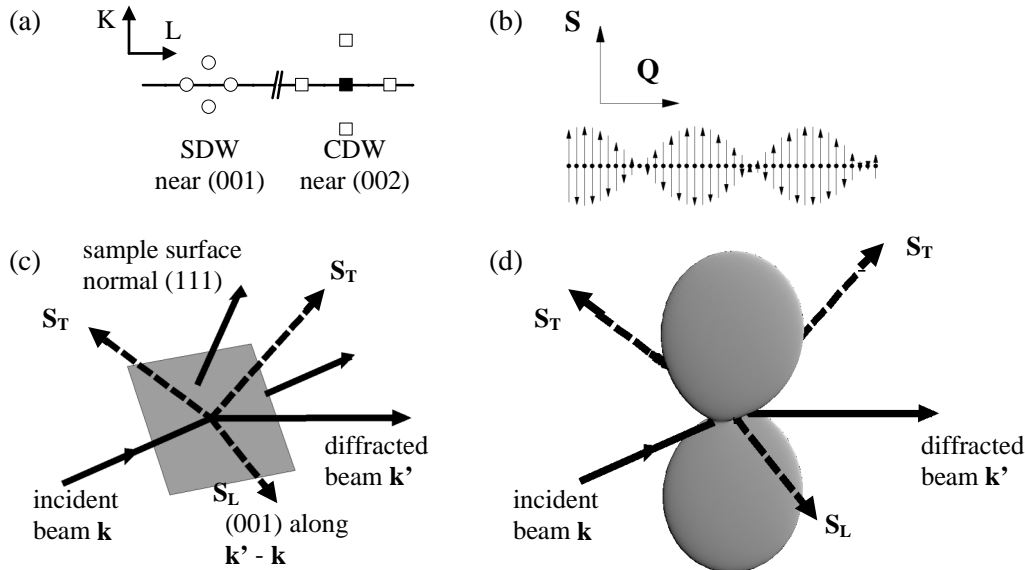


Figure 1 (a) The $(0KL)$ plane of reciprocal space near (001) and (002) , with the positions of the (002) allowed Bragg (solid square), charge density wave satellite (open squares), and spin density wave magnetic satellite (open circles) reflections. (b) The transverse SDW state of Cr with spin polarization S and modulation wavevector Q . The period of the SDW is approximately 20 times the Cr lattice spacing, a_{Cr} . (c) The diffraction geometry for a domain with Q along $[001]$. Dashed lines give the directions for transverse and longitudinal spin polarizations (marked with S_T and S_L respectively) within this domain. (d) The non-resonant scattering cross section varies with the orientation of the spins relative to the incident and diffracted wavevectors. Here the cross section is plotted as a function of direction along with the spin polarizations for the (001) domain shown in part (c). The magnetic cross section for scattering from spins in the longitudinal polarization is reduced by a factor of 30 in comparison to the transverse polarization.

At temperatures above the spin-flip transition at $T_{SF}\approx 120$ K the ordered spins are transverse to the modulation direction in each SDW domain (Figure 1(b)). Upon cooling through T_{SF} , the spin polarization rotates to point along the modulation direction so that the ordered spins exist only in a longitudinally polarized state. The orientations of the transverse and longitudinal spins are shown with the scattering geometry for this experiment in Figure 1(c). In order to saturate the magnetic order parameter to maximize the intensity of the magnetic reflections and to access the temperature regime of the spin-flip transition the sample was cooled using a continuous flow cryostat with incident and diffracted beams passing through a Be dome.

The cross section for non-resonant x-ray scattering in our geometry is proportional to $(\mathbf{S} \cdot (\mathbf{k} \times \mathbf{k}'))^2 + (2 \mathbf{S} \cdot \mathbf{k} \sin^2 \theta)^2$, where θ is the Bragg angle of the magnetic reflection.⁵ A polar plot of the dependence of the cross section on the spin polarization relative to the incident and

diffracted wavevectors is shown in Figure 1(d). The magnetic scattering cross section is dominated by the first term above so that for spin polarizations in the scattering plane the intensity of magnetic scattering drops dramatically. For diffraction from domains with \mathbf{Q} along [001] in our geometry, the cross sections for the two transverse spin polarizations are equal and are a factor of 30 greater than for the longitudinal spin polarization.⁶

We used a single crystal Cr (111) sample in which each of the three possible SDW domains was present as illustrated in room temperature laboratory diffractometer reciprocal space scans through the strain wave peaks at $(2+2\delta, 0, 0)$, $(0, 2+2\delta, 0)$ and $(0, 0, 2+2\delta)$ shown in Figure 2. For these measurements, the incident Cu $\kappa\alpha$ radiation formed a millimeter-scale spot. Strain wave reflections from each possible domain are clearly visible. The small projections of orthogonal strains onto the central peak precluded observation of all three domains around a single allowed Bragg peak.⁶

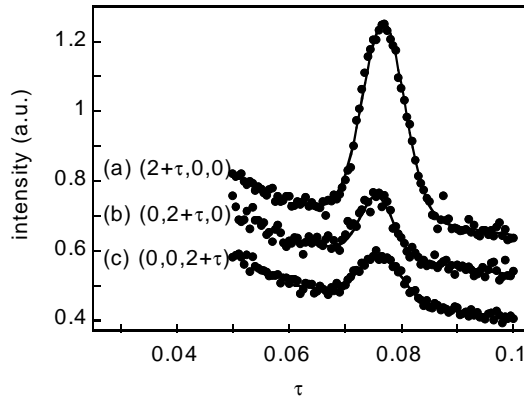


Figure 2 Laboratory diffractometer scans near (a) $(2, 0, 0)$, (b) $(0, 2, 0)$, and (c) $(0, 0, 2)$ for the Cr (111) crystal sample. The solid lines are fits of a Gaussian peak and a monotonically decreasing background. The peaks at $\tau=2\delta=0.075$ arise from the strain wave and demonstrate that domains of each SDW modulation direction exist in this sample.

RESULTS

A map of the intensity of the magnetic $(0, 0, 1-\delta)$ reflection in a $75 \times 75 \mu\text{m}^2$ area of the sample appears in Figure 2(a). To reduce the background due to fluorescence of the sample, images of this magnetic reflection were made with 5.8 keV incident photons, an energy below the onset of absorption at the Cr K shell absorption edge. The same area was also imaged with the strain reflection at $(0, 0, 2-2\delta)$ as shown in Figure 2(b). In order to have nearly the same diffractometer angles for the two reflections, an incident energy of 11.6 keV was used for the strain wave reflection. The sample temperature was 130 K, just above the spin-flip transition in the transverse SDW phase. The same SDW domain appears in both Figure 2(a) and (b) and occupies the majority of each image. The maximum count rates for the two reflections were 10 s^{-1} and 1200 s^{-1} .

The transition between transverse and longitudinal polarization can be observed by making use of the spin-polarization dependence of the non-resonant magnetic x-ray scattering cross section. The images shown in Figure 3 with the sample held at 110 K, below the spin-flip transition, demonstrate the vanishing of the magnetic scattering upon cooling. Although the domains of the SDW modulation direction \mathbf{Q} are unchanged, the magnetic scattering is completely suppressed due to the reduction of the magnetic scattering cross section for spins polarized in the scattering plane. This effect has been employed in studies of spin-flip transition

at the micron scale leading to the observation that the spin-flip transition temperature can vary with position by up to several degrees, even at the scale of a single SDW domain.⁷

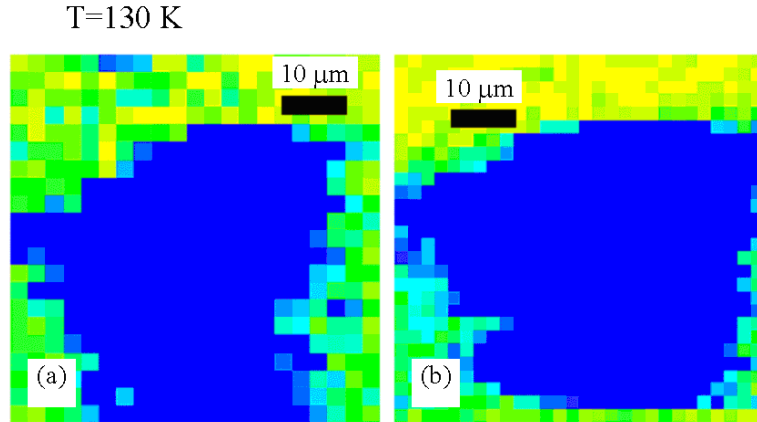


Figure 3 Images at 130 K, in the transverse SDW phase, of the intensity of scattering in the (a) $(0\ 0\ 1-\delta)$ magnetic reflection and (b) $(0\ 0\ 2-2\delta)$ strain wave reflection as the sample was scanned under the microprobe beam. The color scale ranges from bright (lowest intensity) to dark (highest intensity) and was chosen to emphasize the domain contrast.

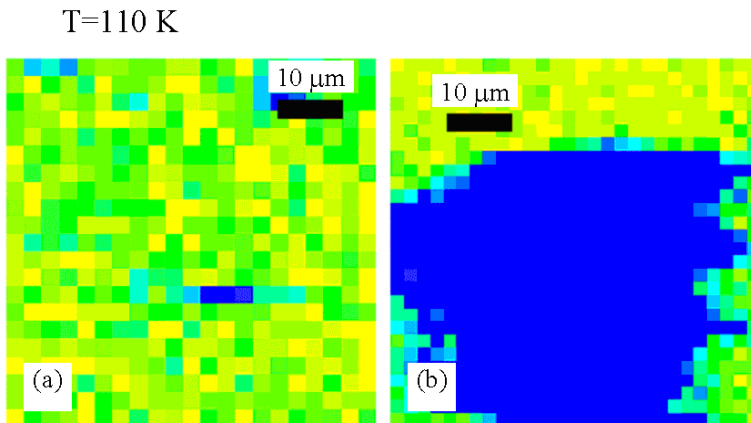


Figure 4 Images formed as in Figure 2, with the sample at 110 K in the longitudinal SDW phase. The intensity of the magnetic reflection (a) has diminished due to the rotation of the spin polarization upon cooling through the spin-flip transition. The strain wave reflection (b) is unchanged.

CONCLUSIONS

Magnetic x-ray microscopy allows antiferromagnetic features to be imaged directly at a length scale that has been impossible with previous techniques. Among the issues that will be addressed by this experimental approach are the role of domain walls of the spin-polarization and modulation direction in phase transitions, the relationship between polarization directions in adjacent domains, and the effects of doping and structural inhomogeneity. Particularly interesting is the question of antiferromagnetic domain polarization domain nucleation upon crossing the spin-flip transition. As devices relying on Cr and other materials have scaled to the

size of single domains and below, these questions have become critically important. X-ray microscopy can likewise be used in conjunction with domain contrast arising from electrical polarization to elucidate phenomena accompanying the switching of ferroelectric domains due to applied electric fields.

ACKNOWLEDGEMENTS

Support for this research by the members of SRI-CAT at the Advanced Photon Source is gratefully acknowledged. Use of the Advanced Photon Source was supported by the U.S. Department of Energy, Office of Science, Office of Basic Energy Sciences, under Contract No. W-31-109-ENG-38.

REFERENCES

- ¹ E. Fawcett, Rev. Mod. Phys. **60** 209 (1988).
- ² M. N. Baibich, J. M. Broto, A. Fert, F. Nguyen Van Dau, F. Petroff, P. Etienne, G. Creuzet, A. Friederich, and J. Chazelas, Phys. Rev. Lett. **61** 2472 (1988); J. Nogués and I. K. Schuller, J. Magn. Magn. Mater. **192** 203 (1999).
- ³ B. Lai, W. Yun, J. Maser, Z. Cai, W. Rodrigues, D. Legnini, Z. Chen, A. A. Krasnoperova, Y. Vladimirska, F. Cerrina, E. Di Fabrizio, and M. Gentili, SPIE Proc. **3449** 133 (1998).
- ⁴ D. Gibbs, K. M. Mohanty, and J. Bohr, Phys. Rev. B **37** (1988).
- ⁵ P. M. Platzman and N. Tzoar, Phys. Rev. B **2** 3556 (1970); M. Blume and D. Gibbs, Phys. Rev. B **37** 1779 (1988).
- ⁶ J. P. Hill, G. Helgesen, and D. Gibbs, Phys. Rev. B **51** 10336 (1995).
- ⁷ P. G. Evans, E. D. Isaacs, G. Aeppli, Z.-H. Cai, and B. Lai, in preparation.